CLOSED FORM EXPRESSIONS FOR PREDICTING MOMENT REDISTRIBUTION IN REINFORCED CONCRETE BEAMS WITH APPLICATION TO CONVENTIONAL CONCRETE AND UHPFRC

[1]Sturm, A.B., [2]Visintin, P. and [3]Oehlers, D.J.

Sturm, A.B., Visintin, P. and Oehlers, D.J., 2020. Closed-form expressions for predicting moment redistribution in reinforced concrete beams with application to conventional concrete and ultrahigh performance fiber reinforced concrete. *Structural Concrete, 21*(4), pp.1577-1596.

ABSTRACT

The redistribution of moment within a statically indeterminate reinforced concrete beam at the ultimate limit state occurs through variations in the flexural rigidities and through the formation of hinges. The phenomena of moment redistribution is used to increase the efficiency of reinforced concrete design by allowing moments to be transferred away from critical cross-sections thereby resulting in lower design moments. To allow for this effect in design, two main approaches are adopted. The first is to perform an elastic analysis and then to adjust the resulting distribution of moment using a codified moment redistribution factor. The second is to apply a plastic analysis allowing for the formation of hinges, and to calculate the rotational requirements at the hinges from first principles. This paper uses fundamental plastic analyses to derive closed form expressions for the hinge rotational requirements for full moment redistribution (that required to achieve the theoretical maximum applied load within the beam based on the moment capacity of sections within the beam). These closed form solutions are then used to quantify the maximum load on a beam when the rotational capacities at a hinge are less than the rotational requirements for full moment redistribution (partial moment redistribution). Closed form solutions are then used to derive moment redistribution factors which do not require semi-mechanical calibration.

INTRODUCTION

Moment redistribution (MR) allows the transfer of moments away from critical cross-sections towards underutilised cross-sections, thereby allowing for a reduction in member size, a reduction in reinforcement congestion, and an increased efficiently of a given design by allowing for the full capacity of statically indeterminate continuous RC beams to be achieved.

Two approaches are available in current design standards to allow for MR while avoiding premature failure due to insufficient rotational capacity of the hinges. The most common approach is to perform an elastic analysis and to then adjust the bending moment diagram according to some MR factor (CEN 2004; ACI 2014; Standards Australia 2018). The second approach is to perform a plastic analysis to determine the rotational demand on the hinges which can then be compared directly to the rotational capacity of the hinges (CEN 2004; fib 2013).

For the first approach, the MR factor is defined as

$$K_{MR} = \frac{M_{el} - M_h}{M_{el}} \quad (1)$$

where M_{el} is the elastic moment and M_h is the actual moment at the position at which the MR factor is being evaluated - typically at the supports. National design standards give different limits for the value of K_{MR} at ultimate which are shown graphically in Fig. 1. For example, AS3600-2018 (Standards Australia 2018) give the maximum MR as a function of the ratio of the neutral axis depth to the effective depth of the section (k_u) and limits MR only to members reinforced with class N reinforcement (rupture strains greater than 0.05). In Eurocode 2 (CEN 2004), the MR factor is a function of $\underline{k_u}$ but is also adjusted for the ductility class of the reinforcement and the concrete strength.

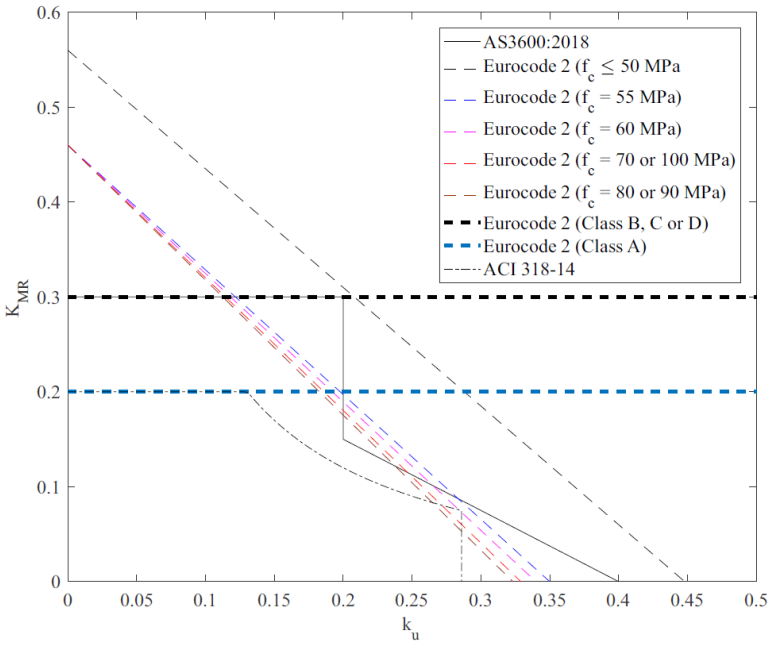

Fig. 1. Code expressions for level of MR

As shown in Fig. 1, K_{MR} is the minimum of the value defined by the concrete strength and the ductility class of the reinforcement. In ACI 318-14 (ACI 2014) the MR factor is given as a function of the strain in the tensile reinforcement, however as the strain at the top fibre is fixed at the ultimate limit, this can also be related to the neutral axis depth.

For AS3600-2018 (Standards Australia 2018), the variation in K_{MR} with k_u was determined by performing a parametric study using a numerical model and then fitting an expression to the results (Gravina & Warner 2003). That is, the relationship is semi-mechanical and calibrated to represent a safe, lower bound prediction. The expressions in the other standards are determined in a similar manner. The observed differences in Fig. 1 are therefore due to the examples considered and the underlying assumptions of the base numerical analysis and the level of conservatism built into each design standard. An identifiable limitation in current practice is, therefore, the inability to extend to applications outside of the original bounds of the parametric study for new materials without repeating the analysis. The expressions in

national codes also consider the quantity of MR to be a section property (the neutral axis depth is only a function of the section from which the moment is being redistributed) and neglect the influence of the member properties such as the variation of the flexural rigidity between the hogging and sagging regions, the span of the beam and the type of loading (Oehlers et al. 2010).

Where the hogging moment is defined as a moment that creates tension on the top face of the beam and a sagging moment is defined as a moment that creates compression on the bottom face of the beam.

The Eurocode 2 (CEN 2004) facilitates plastic analysis by providing relationships for the rotational capacity as a function of the neutral axis depth, concrete strength and ductility class of the reinforcement. However, the rotation requirement at the hinges needs to be determined from first principles (CEN 2004).

The goal of this paper is therefore to derive mechanics solutions that can quantify the level of MR, this is done with the aim of creating a single generic approach that can be applied to both conventional concretes and emerging materials such as ultra-high performance fibre reinforced concrete (UHPFRC). The solutions are presented in such a way as to provide designers with a choice in terms of implementation approach. They can be implemented by imposing a desired bending moment distribution and solving for the necessary rotational capacities of the hinges to achieve the imposed moment distribution. Alternatively, they can be applied by quantifying the maximum load that a member can resist based on the rotational capacity of the hinges. To allow for the first form of analysis closed form solutions are derived for the rotation at the hinges required to achieve full MR, and to allow for the second form of analysis these solutions are manipulated for application when a beam hinge has insufficient rotational capacity to achieve full MR, that is partial MR. Finally, the expressions derived are compared to experimental results for conventional reinforced concrete beams and current code approaches.

To show the generic nature of the approach, the expressions derived are then used to quantify MR in UHPFRC beams.

MECHANICS OF MOMENT REDISTRIBUTION

Moment redistribution at the ultimate limit state

Let us define the mechanics of MR in this paper as the quantification of the maximum load a statically indeterminate beam can withstand as well as the rotation required at any hinges that may have formed to achieve this maximum load. At this maximum load, the beam has not collapsed. However, after this maximum load is attained, any further applied deformations may cause the formation of more hinges which may form at the maximum load or at lower applied loads which then leads to a collapse mechanism.

To allow the derivation of closed form solutions for the MR factors, we will define an elastic analysis of a statically indeterminate beam as an analysis of a beam with a constant flexural rigidity (EI), and in which the material remains elastic and hinges have not formed. Hence any deviation from this elastic distribution of moment is MR and which can now be caused by variations in the flexural rigidities along the beam and the formation of hinges.

Moment-rotation relationship of reinforced concrete

A typical moment-rotation relationship of an RC hinge is shown in Fig. 2 which, for the closed form analyses, is idealised as a linear rising branch of flexural rigidity EI, a plastic plateau at M_h of a rotational capacity θ_h and after which there is a rapidly descending branch. Here the rotational capacity θ_h is defined as the maximum possible rotation less the rotation associated with the rising branch. This definition is imposed as it allows the total rotation be defined as the summation of the rotation due to the flexural rigidity EI, and a point rotation representing the contribution of the plateau (hinge rotation).

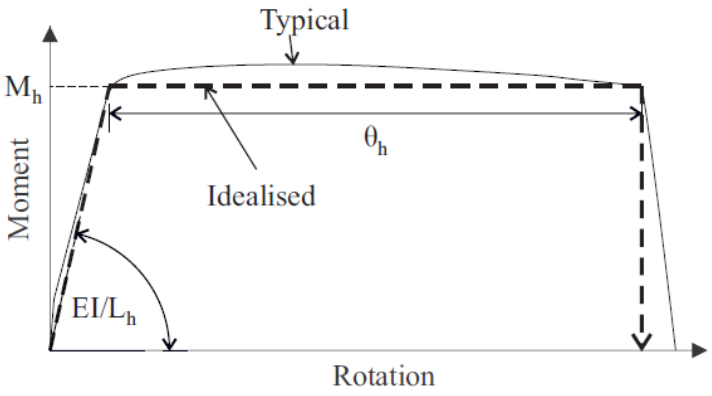

Fig. 2. Typical moment rotation relationship for reinforced concrete hinge

A number of different approaches are available in the literature for predicting the moment-rotation of a hinge in reinforced concrete. These include segmental analysis approaches that give the moment-rotation directly (Bachmann 1971; Bigaj 1999; Gravina 2002; Haskett et al. 2009; Visintin et al. 2012) and which have been extended to fibre reinforced concrete (Schumacher 2006; Visintin & Oehlers 2018), as well as hinge length approaches that allow the moment-rotation to be determined from the moment-curvature relationship (see the review of Panagiotakos & Fardis 2001).

Importantly, softening moment-rotation relationships may occur for FRC and UHPFRC, and these can be accommodated using the idealised representation in Fig. 2. This is achieved by the designer determining how far they are willing to allow the moment to reduce after achieving the peak moment. At this point M_h is the moment reduced by softening and θ_h is equal to the rotation to achieve this reduced moment (less the rotation due to the rising branch).

Moment redistribution mechanism

To discuss MR, consider the continuous beam with a span of L subjected to a uniformly distributed load (UDL) w in Fig. 3(a). The hinge rotation at the support due to w is given by θ_{hog} and the hinge rotation at the point of maximum moment in the midspan is given by θ_{sag}, The moments at each location are M_{hog} and M_{sag}, respectively. The elastic distribution of moment is illustrated in Fig. 3(b) where the moment at the midspan is half that at the supports. This represents the distribution of moment before the moment capacity is reached at any point of the beam (neglecting MR due to variations in EI).

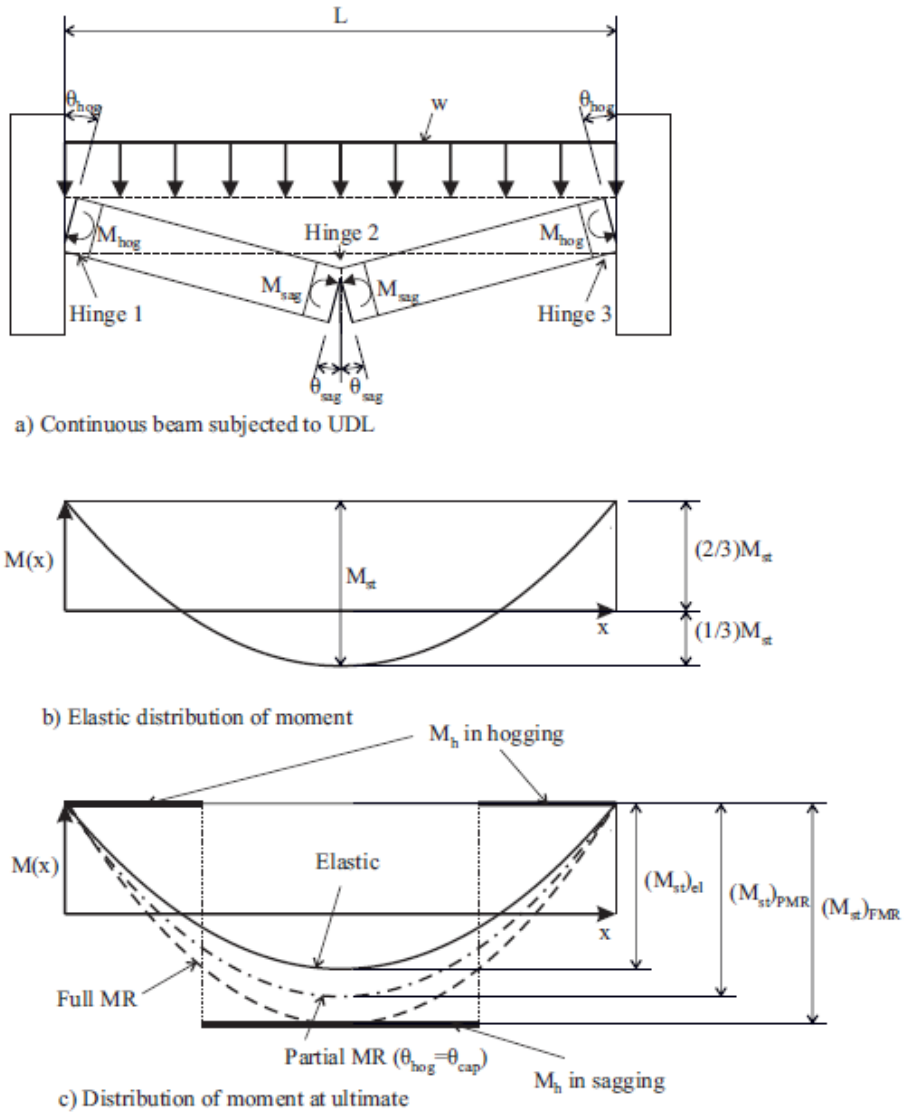

Fig. 3. Reinforced concrete beam at ultimate loading condition

In Fig. 3(c), the hinge moment capacities M_h in the hogging and sagging regions are illustrated. Before a hinge has formed M_{hog} or M_{sag} are less than M_h and after the hinge had formed they are equal to M_h. As the applied load increases, the moment capacity is eventually reached at some point along the beam. If the moment capacity is first reached at the supports, then the bending moment distribution is given by the solid line in Fig. 3(c). For a brittle beam with no rotational capacity this represents the ultimate load.

Hinges in reinforced concrete members have some ductility and therefore rotation can occur to allow the moment to redistribute from a plastic region to another (stiffer) location along the beam where the moment capacity has not yet been reached. When these locations reach their moment capacities full MR has been achieved. For a continuous beam, this occurs when the hinge moment capacity has been reached at three cross-sections: both supports and the point of maximum sagging moment at the midspan. At this point, the ultimate load is reached and the distribution of moment is given by the dashed line in Fig. 3(c). This represents the maximum possible load that could be applied to the beam assuming sufficient rotational capacity exists at the hinges at the supports, as shown by the increase in the static moment $(M_{st})_{FMR}>(M_{st})_{el}$. This situation, where the moment capacities of the sections are achieved and consequently any increase in rotational capacity does not result in an increase in MR, is referred to as full MR.

The distribution of moment associated with full MR can only be achieved if the rotational capacity at the hinges is not exceeded. If the rotational capacity is exceeded at any of the hinges, then the applied load w at which this occurs is the maximum capacity of the beam. In this case, the bending moment distribution would be intermediate between those corresponding to the elastic and full MR loads, that is, the dashed-dotted line in Fig. 3(c). This is referred to as partial MR because the level of MR is intermediate and lies between the elastic case and full MR. For

partial MR $(M_{st})_{el}<(M_{st})_{PMR}<(M_{st})_{FMR}$, that is the ultimate load w is intermediate between that for the elastic and full MR cases.

In the subsequent section, expressions are developed for quantifying the rotational requirements at the hinges as a function of the applied bending moment distribution. Hence a comparison of a section's rotational capacity with the member rotational requirement at that section will determine whether the full MR can be achieved or premature failure occurs due to a lack of ductility that is partial MR.

ROTATIONAL REQUIREMENT FOR FULL MR

Consider the continuous beam with a UDL in Fig. 4(a). This beam is subject to the bending moment distribution in Fig. 4(b) which may cause some rotation at the hinges. To determine these rotations, consider the deflection at the right hand when and the right hand support is removed and the bending moment in Fig. 4(b) is applied. This causes a deflection upwards or downwards as shown in Fig. 4(c). This deflection is referred to as the elastic deflection y_{el} as this is the deflection due to the curvature distributed along the beam. However as the total deflection is required to be zero at the right hand support position, an equal and opposite deflection has to be applied to counteract this elastic deflection y_h. This deflection is generated by the hinges. The total deflection can therefore be written as

$$y = 0 = y_{el} + y_h \tag{2}$$

To determine $\underline{y_h}$ the distribution of hinges needs to be considered. There are three possible hinge locations for a continuous beam: left hand support, right hand support and position of the maximum sagging moment as shown in Fig. 4(a). Next, consider that at the instant before full MR is achieved there are two hinges in the beam. Applying these constraints there are three situations that can occur: (i) hinges at the supports as shown in Fig. 4(d-e); (ii) hinges at the left hand support and the position of maximum sagging moment as shown in Fig. 4(f-g) and

(iii) hinge at the position of maximum sagging moment and the right hand support as shown in Fig. 4(h-i).

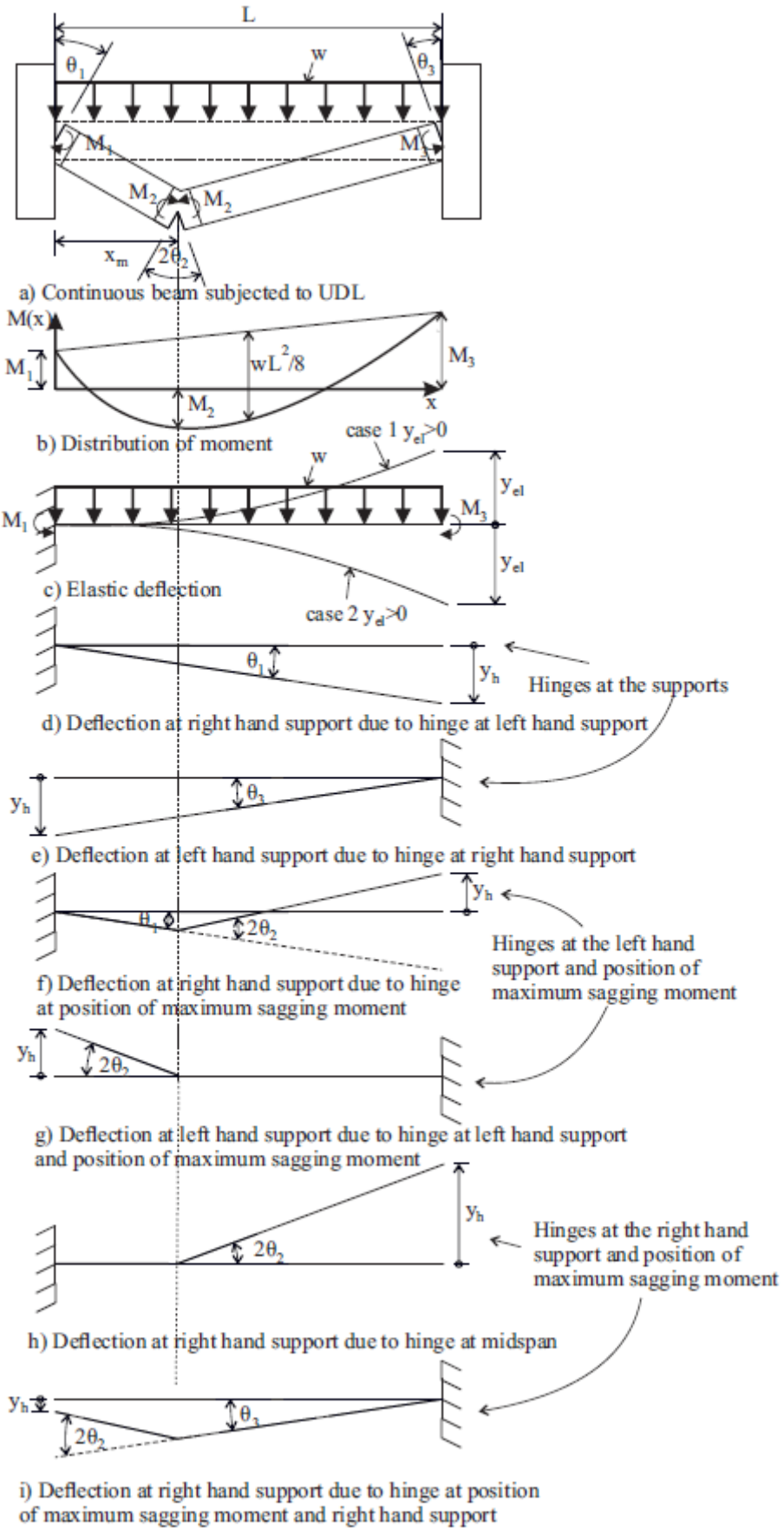

Fig. 4. Elastic and hinge deflections

To decide which situation applies, first release the right hand support in Fig. 4(a) and calculate y_{el} at this position. Next release the left hand support and calculate y_{el} at that position, paying attention to the direction of the deflection. If the elastic deflections y_{el} calculated at the left and right hand supports are both upwards, then the hinges form at the supports to counteract this deflection. The resulting hinge deflections, as shown in Fig. 4(d-e), are given as

$$y_h(0) = \theta_3 L \tag{3}$$

$$y_h(L) = \theta_1 L \tag{4}$$

If the elastic deflection y_{el} at the left hand support is upwards while the elastic deflection y_{el} at the right hand support is downwards, then hinges form at the position of the maximum sagging moment and the right hand support. From Fig. 4(h-i), the resulting deflections are given as

$$y_h(0) = \theta_3 L + 2\theta_2 x_m \tag{5}$$

$$y_h(L) = 2\theta_2 (L - x_m) \tag{6}$$

Conversely if the deflection y_{el} is downwards at the left hand support and upwards at the right hand support, then the hinges form at the left hand support and the position of the maximum sagging moment. That is

$$y_h(0) = 2\theta_2 x_m \tag{7}$$

$$y_h(L) = \theta_1 L + 2\theta_2 (L - x_m) \tag{8}$$

Finally, the last case to consider is when the deflection is downwards at both supports. In this case, first calculate the position of maximum sagging moment rotation required to counteract the hinge deflection at the left hand support and that required to counteract the hinge deflection at the right hand support, ignoring any hinges at the supports. That is

$$(\theta_2)_0 = -\frac{y_{el}(0)}{2x_m} \tag{9}$$

$$(\theta_2)_L = -\frac{y_{el}(L)}{2(L-x_m)} \tag{10}$$

The actual hinge rotation at the position of maximum sagging moment is given by the maximum of Eq. (9) and Eq. (10). For example when $(\theta_2)_0 > (\theta_2)_L$, then the additional hinge forms at left hand support. Conversely when $(\theta_2)_L < (\theta_2)_0$, then the additional hinge forms at the right hand support. In the first case, the hinge deflections are given by Eqs. (7-8) and in the second case the hinge deflections are given by Eqs. (9-10). These different cases are summarised in Table 1 where 1 is the hinge at left hand support, 2 is the hinge at the position of maximum sagging moment and 3 is the hinge at the right hand support.

Table 1: Hinge locations

		$y_{el}(0)>0$	$y_{el}(0)<0$
$y_{el}(L)>0$		1,3 Eq. (3-4)	1,2 Eq. (7-8)
$y_{el}(L)<0$	$(\theta_2)_0>(\theta_2)_L$	2,3 Eq. (5-6)	1,2 Eq. (7-8)
	$(\theta_2)_L<(\theta_2)_0$		2,3 Eq. (5-6)

The next step is to evaluate the elastic deflection y_{el} when the right hand support is released. The variation in curvature is given by the following expression

$$\chi(x) = \frac{M(x)}{EI_i};\ x_{i-1} < x < x_i;\ i \in (1, N) \tag{11}$$

where the beam is divided into N segments where EI_i is the flexural rigidity within the given segment as illustrated in Fig. 5.

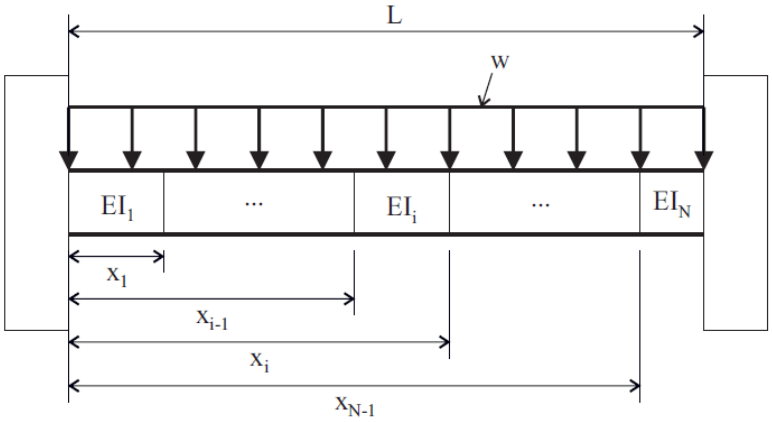

Fig. 5 Flexural rigidity of beam

For a continuous beam subjected to a UDL, the bending moment in Fig. 4(b) is

$$M(x) = w\left(\frac{Lx}{2} - \frac{x^2}{2}\right) + M_1\left(1 - \frac{x}{L}\right) + M_3\left(\frac{x}{L}\right) \tag{12}$$

and the maximum moment occurs at a distance x_m from the left hand support, where the derivative of Eq. (12) is equal to zero, that is

$$\frac{dM}{dx} = 0 = \frac{wL}{2} - wx_m - \frac{M_1}{L} + \frac{M_3}{L} \tag{13}$$

Rearranging Eq. (13) gives the position of the maximum moment as

$$x_m = \frac{L}{2} - \frac{M_1 - M_3}{wL} \tag{14}$$

which also gives the location of the maximum sagging moment, which is a location a hinge may form.

Substituting Eq. (12) into Eq. (11) gives the variation in curvature as a function of position

$$\chi(x) = \frac{w}{EI_i}\left(\frac{Lx}{2} - \frac{x^2}{2}\right) + \frac{M_1}{EI_i}\left(1 - \frac{x}{L}\right) + \frac{M_3}{EI_i}\left(\frac{x}{L}\right);\ x_{i-1} < x < x_i;\ i \in (1, N) \quad (15)$$

Integrating gives the variation in the elastic rotation of the beam, which is the portion of the rotation due to the curvature of the beam between the hinges induced by the applied loading

$$\theta_{el}(x) = \frac{w}{EI_i}\left(\frac{Lx^2}{4} - \frac{x^3}{6}\right) + \frac{M_1}{EI_i}\left(x - \frac{x^2}{2L}\right) + \frac{M_3}{EI_i}\left(\frac{x^2}{2L}\right) + (c_1)_i;\ x_{i-1} < x < x_i;\ i \in (1, N) \quad (16)$$

At the left hand support, the rotation is zero (for the case where the right hand support is released), hence

$$\theta_{el}(0) = 0 = (c_1)_1 \quad (17)$$

The rotation is also continuous across segment boundaries, therefore

$$\theta_{el}(x_{i+1}) = \frac{w}{EI_i}\left(\frac{Lx_{i+1}^2}{4} - \frac{x_{i+1}^3}{6}\right) + \frac{M_1}{EI_i}\left(x_{i+1} - \frac{{x_{i+1}}^2}{2L}\right) + \frac{M_3}{EI_i}\left(\frac{{x_{i+1}}^2}{2L}\right) + (c_1)_i = \frac{w}{EI_{i+1}}\left(\frac{Lx_{i+1}^2}{4} - \frac{x_{i+1}^3}{6}\right) + \frac{M_1}{EI_{i+1}}\left(x_{i+1} - \frac{{x_{i+1}}^2}{2L}\right) + \frac{M_3}{EI_{i+1}}\left(\frac{{x_{i+1}}^2}{2L}\right) + (c_1)_{i+1} \quad (18)$$

Rearranging gives

$$(c_1)_{i+1} - (c_1)_i = w\left(\frac{1}{EI_i} - \frac{1}{EI_{i+1}}\right)\left(\frac{Lx_{i+1}^2}{4} - \frac{x_{i+1}^3}{6}\right) + M_1\left(\frac{1}{EI_i} - \frac{1}{EI_{i+1}}\right)\left(x_{i+1} - \frac{{x_{i+1}}^2}{2L}\right) + M_3\left(\frac{1}{EI_i} - \frac{1}{EI_{i+1}}\right)\left(\frac{{x_{i+1}}^2}{2L}\right) \quad (19)$$

Integrating the elastic rotation gives the elastic deflection in Fig. 4(c)

$$y_{el}(x) = \frac{w}{EI_i}\left(\frac{Lx^3}{12} - \frac{x^4}{24}\right) + \frac{M_1}{EI_i}\left(\frac{x^2}{2} - \frac{x^3}{6L}\right) + \frac{M_3}{EI_i}\left(\frac{x^3}{6L}\right) + (c_1)_i x + (c_2)_i;\ x_{i-1} < x < x_i;\ i \in (1, N) \quad (20)$$

At the right hand support the deflection is zero, hence

$$y_{el}(0) = 0 = (c_2)_1 \quad (21)$$

and given the deflection is continuous across segment boundaries

$$y_{el}(x_{i+1}) = \frac{w}{EI_i}\left(\frac{Lx_{i+1}^3}{12} - \frac{x_{i+1}^4}{24}\right) + \frac{M_1}{EI_i}\left(\frac{{x_{i+1}}^2}{2} - \frac{{x_{i+1}}^3}{6L}\right) + \frac{M_3}{EI_i}\left(\frac{{x_{i+1}}^3}{6L}\right) + (c_1)_i x_{i+1} + (c_2)_i =$$

$$\frac{wL{x_{i+1}}^3}{12EI_{i+1}} - \frac{w{x_{i+1}}^4}{24EI_{i+1}} + \frac{M_1}{EI_{i+1}}\left(\frac{{x_{i+1}}^2}{2} - \frac{{x_{i+1}}^3}{6L}\right) + \frac{M_3}{EI_{i+1}}\left(\frac{{x_{i+1}}^3}{6L}\right) + (c_1)_{i+1} x_{i+1} + (c_2)_{i+1} \quad (22)$$

Rearranging Eq. (22) gives

$$(c_2)_{i+1} - (c_2)_i = w\left(\frac{1}{EI_i} - \frac{1}{EI_{i+1}}\right)\left(\frac{Lx_{i+1}^3}{12} - \frac{x_{i+1}^4}{24}\right) + M_1\left(\frac{1}{EI_i} - \frac{1}{EI_{i+1}}\right)\left(\frac{{x_{i+1}}^2}{2} - \frac{{x_{i+1}}^3}{6L}\right) +$$

$$M_3\left(\frac{1}{EI_i} - \frac{1}{EI_{i+1}}\right)\left(\frac{{x_{i+1}}^3}{6L}\right) - [(c_1)_{i+1} - (c_1)_i]x_{i+1} = -w\left(\frac{1}{EI_i} - \frac{1}{EI_{i+1}}\right)\left(\frac{Lx_{i+1}^3}{6} - \frac{x_{i+1}^4}{8}\right) -$$

$$M_1\left(\frac{1}{EI_i} - \frac{1}{EI_{i+1}}\right)\left(\frac{{x_{i+1}}^2}{2} - \frac{{x_{i+1}}^3}{3L}\right) - M_3\left(\frac{1}{EI_i} - \frac{1}{EI_{i+1}}\right)\left(\frac{{x_{i+1}}^3}{3L}\right) \quad (23)$$

From Eq. (12), the elastic deflection at the right hand support is given by

$$y_{el}(L) = \frac{wL^4}{24EI_N} + \frac{M_1L^2}{3EI_N} + \frac{M_3L^2}{6EI_N} + (c_1)_N L + (c_2)_N = a_1 w + a_2 M_1 + a_3 M_3 \quad (24)$$

where

$$a_1 = \frac{L^4}{24EI_N} + \sum_{i=1}^{N-1}\left(\frac{1}{EI_i} - \frac{1}{EI_{i+1}}\right)\left(\frac{L^2x_{i+1}^2}{4} - \frac{Lx_{i+1}^3}{3} + \frac{x_{i+1}^4}{8}\right) \quad (25a)$$

$$a_2 = \frac{L^2}{3EI_N} + \sum_{i=1}^{N-1}\left(\frac{1}{EI_i} - \frac{1}{EI_{i+1}}\right)\left(Lx_{i+1} - x_{i+1}^2 + \frac{x_{i+1}^3}{3L}\right) \quad (25b)$$

$$a_3 = \frac{L^3}{6EI_N} + \sum_{i=1}^{N-1}\left(\frac{1}{EI_i} - \frac{1}{EI_{i+1}}\right)\left(\frac{x_{i+1}^2}{2} - \frac{x_{i+1}^3}{3L}\right) \quad (25c)$$

Following the same procedure, the elastic deflection at the left hand support when this is released is given by

$$\theta_3 L + 2\theta_2 x_m = -y_{el}(0) = -[a_1{}'w + a_2{}'M_1 + a_3{}'M_3] \quad (26)$$

where

$$a_1' = \frac{L^4}{24EI_1} - \sum_{i=1}^{N-1}\left(\frac{1}{EI_i} - \frac{1}{EI_{i+1}}\right)\left(\frac{L^2 x'^2_{i+1}}{4} - \frac{L x'^3_{i+1}}{3} + \frac{x'^4_{i+1}}{8}\right) \tag{27a}$$

$$a_2' = \frac{L^2}{6EI_1} - \sum_{i=1}^{N-1}\left(\frac{1}{EI_i} - \frac{1}{EI_{i+1}}\right)\left(\frac{x'^2_{i+1}}{2} - \frac{x'^3_{i+1}}{3L}\right) \tag{27b}$$

$$a_3{}' = \frac{L^2}{3EI_1} - \sum_{i=1}^{N-1}\left(\frac{1}{EI_i} - \frac{1}{EI_{i+1}}\right)\left(L x'_{i+1} - x'^2_{i+1} + \frac{x'^3_{i+1}}{3L}\right) \tag{27c}$$

where the position with respect to the right hand support is given by

$$x' = L - x \tag{28}$$

From Eqs. (24) and (26), the elastic deflections at the supports can be calculated. Table 1 can then be used to determine the position of the hinges, and therefore the correct expressions for the hinge deflections can be selected from Eqs. (3-8). Hence by substituting the hinge and elastic deflections into Eq. (2) and rearranging, the rotations can be determined. From this and for the case in Fig. 4(d-e)

$$\theta_1 = -\frac{y_{el}(L)}{L} \tag{29}$$

$$\theta_3 = -\frac{y_{el}(0)}{L} \tag{30}$$

For the case in Figs. 4(f-g)

$$\theta_2 = -\frac{y_{el}(0)}{2x_m} \tag{31}$$

$$\theta_1 = -\frac{y_{el}(L)}{L} - 2\theta_2\left(1 - \frac{x_m}{L}\right) \tag{32}$$

For the case in Figs. 4(h-i)

$$\theta_2 = -\frac{y_{el}(L)}{2(L-x_m)} \tag{33}$$

$$\theta_3 = -\frac{y_{el}(0)}{L} - 2\theta_2\frac{x_m}{L} \tag{34}$$

The suggested workflow, for applying this approach to design a beam for moment redistribution, is given in Fig. 6.

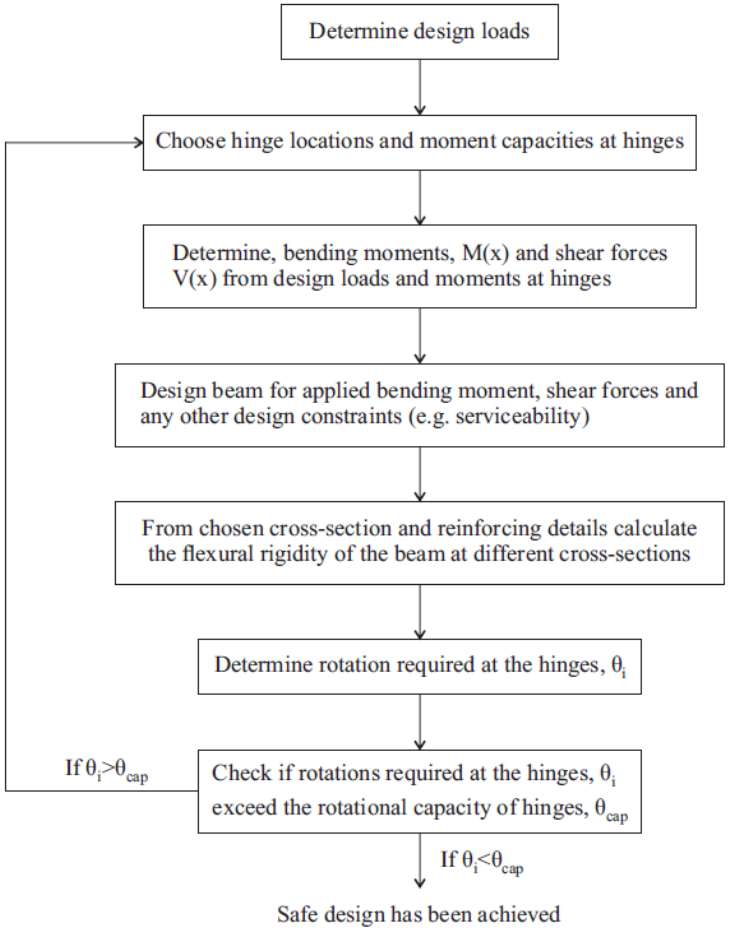

Fig. 6. Design procedure to allow sufficient MR

In this example, a continuous beam with a UDL has been considered, however, other support and loading arrangements can be considered as well. For example a propped cantilever can be considered by setting the moment at the simple support to zero. The required rotation for a continuous beam with a point load is also given in Appendix A.

APPLIED LOAD FOR PARTIAL MR

If insufficient rotational capacity is available at the hinges such that full MR cannot be achieved, the expressions in the previous section can be adapted to calculate the load that can be achieved given the available rotational capacity, that is partial MR. To do this, first a partial mechanism needs to be identified. This can be done by inspecting the elastic distribution of moment to find the location of the first hinge. From this, three partial mechanisms involving a single hinge can be identified: (i) hinge at left hand support; (ii) hinge at right hand support; (iii) hinge at position of maximum sagging moment.

Hinge at left hand support

Substituting Eq. (24) and Eq. (4) into Eq. (2) and rearranging gives the following

$$\theta_1 L = -[a_1 w + a_2 M_1 + a_3 M_3] \tag{35}$$

and as the hinge deflection at the left hand support due to a rotation at this support is zero, the following is obtained by substituting Eq. (26) into Eq. (2)

$$0 = -[a_1' w + a_2' M_1 + a_3' M_3] \tag{36}$$

Solving Eqs. (35) and (36) gives the following applied load and moment at the right hand support

$$M_3 = \frac{M_1(a_2 a_1' - a_1 a_2') + \theta_1 L a_1'}{a_1 a_3' - a_3 a_1'} \tag{37}$$

$$w = -\frac{a_2 M_1 + a_3 M_3 + \theta_1 L}{a_1} \tag{38}$$

Hinge at right hand support

Similarly to the previous case but for a hinge at the right hand support, the moment at the left hand support and the applied load is given by

$$M_3 = \frac{M_3(a_3 a_1' - a_1 a_3') - \theta_3 L a_1}{a_1 a_2' - a_2 a_1'} \tag{39}$$

$$w = -\frac{a_2 M_1 + a_3 M_3}{a_1} \tag{40}$$

Hinge at the position of maximum sagging moment

To solve this, three simultaneous equations are required. Substituting Eq. (24) and Eq. (6) into Eq. (2) gives

$$2\theta_2(L - x_m) = -[a_1 w + a_2 M_1 + a_3 M_3] \tag{41}$$

From Eq. (26) and Eq. (7)

$$2\theta_2 x_m = -[a_1' w + a_2' M_1 + a_3' M_3] \tag{42}$$

From Eq. (12)

$$M(x_m) = M_2 = w\left(\frac{L x_m}{2} - \frac{x_m^2}{2}\right) + M_1\left(1 - \frac{x_m}{L}\right) + M_3\left(\frac{x_m}{L}\right) \tag{43}$$

x_m is determined from the distribution of moment immediately before the formation of the hinge at the position of maximum sagging moment. Solving gives

$$M_3 = \frac{a_2' M_2 + 2\theta_2\left(x_m - \frac{x_m^2}{L}\right)}{-a_3' + (a_2' + a_3')\frac{x_m}{L}} \tag{44}$$

$$M_1 = \frac{a_3 M_2 + 2\theta_2\left(x_m - \frac{x_m^2}{L}\right)}{a_3 - (a_2 + a_3)\frac{x_m}{L}} \tag{45}$$

$$w = \frac{M_2}{\frac{L x_m}{2} - \frac{x_m^2}{2}} - M_1 \frac{1 - \frac{x_m}{L}}{\frac{L x_m}{2} - \frac{x_m^2}{2}} - M_3 \frac{\frac{x_m}{L}}{\frac{L x_m}{2} - \frac{x_m^2}{2}} \tag{46}$$

After calculating the distribution of moments, the moments at the other possible hinge locations need to be checked. If the hinge moment at any hinge location is exceeded, a partial hinge mechanism with two hinges needs to be considered.

Hinge at left hand support and right hand supports

For this case the uniformly distributed load is given by Eq. (38).

Hinge at the position of maximum sagging moment and left hand support

Substituting Eq. (24) and Eq. (8) into Eq. (1) gives

$$\theta_1 L + 2\theta_2(L - x_m) = -[a_1 w + a_2 M_1 + a_3 M_3] \tag{47}$$

Solving Eq. (47) and Eq. (42)

$$M_3 = \frac{(a_2 a_1' - a_1 a_2')M_1 + \theta_1 L a_1' + 2\theta_2[L a_1' - x_m(a_1 + a_1')]}{a_1 a_3' - a_3 a_1'} \tag{48}$$

And the applied load is given by Eq. (46).

Hinge at maximum sagging moment and right hand support

Similarly for a hinge at the position of maximum sagging moment and right hand support, the moment at the left hand support is given by

$$M_1 = \frac{(a_3 a_1' - a_1 a_3')M_1 - \theta_3 L a_1 + 2\theta_2[L a_1' - x_m(a_1 + a_1')]}{a_1 a_3' - a_3 a_1'} \tag{49}$$

And the applied load is given by Eq. (46).

Hinges at maximum sagging moment, left hand support and right hand support

If after trying a two hinge mechanism, the moment still exceeds the hinge moment at the third hinge location, then a three hinge mechanism needs to be considered. This corresponds to the distribution of moment determined using plastic limit analysis. Rearranging Eq. (30) at this stage gives the applied load as

$$w = \frac{-M_1\left(1 - \frac{x_m}{L}\right) + M_2 - M_3\left(\frac{x_m}{L}\right)}{\frac{L x_m}{2} - \frac{x_m^2}{2}} \tag{50}$$

MOMENT REDISTRIBUTION FACTORS

In this section, a single value of flexural rigidity is attributed to the hogging regions of a beam and a single value is attributed to the sagging region as this is most commonly encountered in design (where the reinforcement ratio is different in each region). Simple expressions are derived for the commonly encountered design cases in Fig. 7. Solutions for other situations are possible. For example they could be derived for all the situations described in the previous section, however, the solutions are complex and have limited applicability and instead the expressions in the previous section could be applied directly.

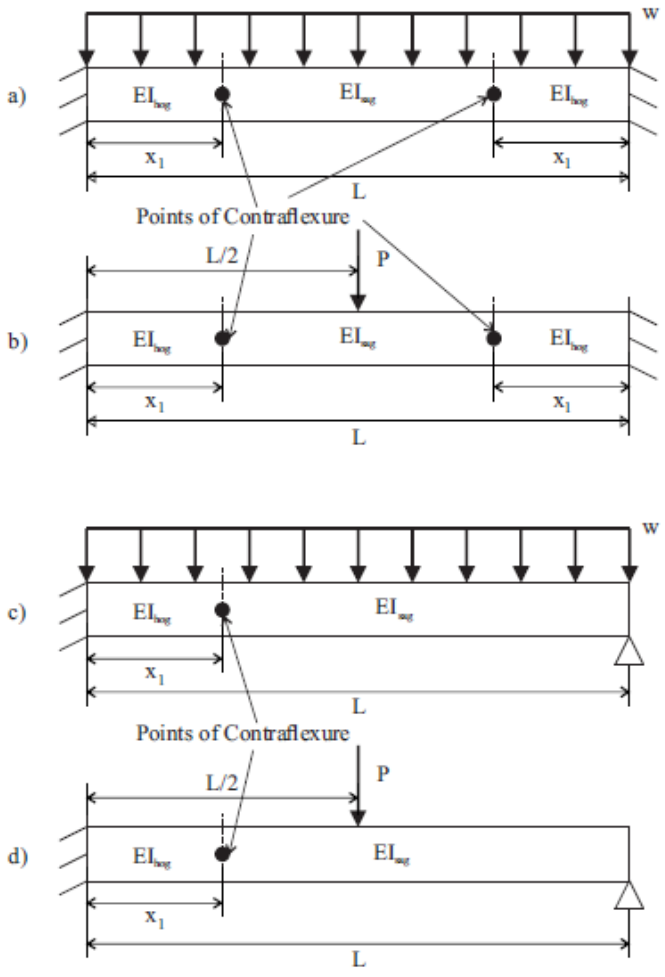

Fig. 7. Cases for simplified expressions; a) continuous beam with identical end moments and UDL; b) continuous beam with identical end moments and central point load; c) propped cantilever with UDL; d) propped cantilever with point load

Hinge at support

Consider the continuous beam in Fig. 7(a) with equal end moments and subject to a UDL. Let $EI_{hog}=EI_1=EI_3$, $EI_{sag}=EI_2$, $M_{hog}=M_1=M_3$ and $\theta_{hog}=\theta_1=\theta_3$. Hence from Eq. (35), the uniformly distributed load is

$$w = -\theta_{hog}\left(\frac{L}{a_1}\right) - M_{hog}\left(\frac{a_2+a_3}{a_1}\right) \tag{51}$$

The elastic moment at the support is then given by

$$M_{el} = -\frac{wL^2}{12} = \frac{L^2}{12a_1}\left[\theta_{hog}L + M_{hog}(a_2+a_3)\right] = \frac{\theta_{hog}L + M_{hog}\left[\frac{L^2}{2EI_{sag}} + \left(\frac{1}{EI_{hog}} - \frac{1}{EI_{sag}}\right)Lx_1\right]}{\frac{L^2}{2EI_{sag}} + \left(\frac{1}{EI_{hog}} - \frac{1}{EI_{sag}}\right)\left(3x_1^2 - \frac{2x_1^3}{L}\right)} \tag{52}$$

And from Eq. (1), the MR factor at the support is given as

$$K_{MR,hog} = \frac{1 + \frac{M_{hog}}{\theta_{hog}}\left(\frac{1}{EI_{hog}} - \frac{1}{EI_{sag}}\right)\left(x_1 - \frac{3x_1^2}{L} + \frac{2x_1^3}{L^2}\right)}{1 + \frac{M_{hog}}{\theta_{hog}}\left[\frac{L}{2EI_{sag}} + \left(\frac{1}{EI_{hog}} - \frac{1}{EI_{sag}}\right)x_1\right]} \tag{53}$$

Similar expressions can be derived for other loading conditions, which have the following general form

$$K_{MR,hog} = \frac{1 + \frac{M_{hog}}{\theta_{hog}}L\left(\frac{1}{EI_{hog}} - \frac{1}{EI_{sag}}\right)b_1}{1 + \frac{M_{hog}}{\theta_{hog}}L\left[b_2\frac{1}{EI_{sag}} + \left(\frac{1}{EI_{hog}} - \frac{1}{EI_{sag}}\right)b_3\right]} \tag{54}$$

where b_1, b_2 and b_3 are given in Table 2 and in which $\xi=x_1/L$. This expression gives the moment redistribution at the support when the rotational capacity of the hinge at the support is achieved. This corresponds to partial MR as discussed earlier. However, there is an upper limit on Eq. (54). If the moment at both supports and at the midspan are equal to their hinge moment capacities, then no additional moment redistribution can occur even if the rotation at the hinges is less than the rotational capacity of the hinges. This corresponds to full MR and in a

subsequent section an expression for this upper limit is determined using a basic plastic analysis.

As a simplification, b_1 and b_3 can be approximated using the elastic point of contraflexure as shown in Table 3.

Table 2 MR Coefficients for Hinge at Support

	$\mathbf{b_1}$	$\mathbf{b_2}$	$\mathbf{b_3}$
Continuous beam with equal end moments and UDL	$\xi - 3\xi^2 + 2\xi^3$	1/2	ξ
Continuous beam with equal end moments and central point load	$\xi - 2\xi^2$	1/2	ξ
Propped cantilever with UDL	$\xi - 3\xi^2 + 3\xi^3 - \xi^4$	1/3	$\xi - \xi^2 + \frac{1}{3}\xi^3$
Propped cantilever with central point load	$\xi - \frac{7}{3}\xi^2 + \frac{11}{9}\xi^3$	1/3	$\xi - \xi^2 + \frac{1}{3}\xi^3$

Table 3 Approximate MR Coefficients for a Hinge at the Support

	$\mathbf{b_1}$	$\mathbf{b_3}$
Continuous beam with equal end moments and UDL (ξ =0.211)	0.0962	0.211
Continuous beam with equal end moments and central point load (ξ =0.25)	0.125	0.25
Propped cantilever with UDL (ξ =0.25)	0.106	0.193
Propped cantilever with central point load (ξ =3/11)	0.124	0.205

Hinge at the midspan

Similar expressions can also be derived if the hinge is assumed to form in the midspan. From Eq. (41) setting $\theta_2=\theta_{sag}$ and $x_2 = L/2$ gives the following for the beam in Fig. 7(a)

$$\theta_{sag} = -w\left(\frac{a_1}{L}\right) - M_{hog}\left(\frac{a_2+a_3}{L}\right) \tag{55}$$

From Eq. (12), the midspan moment is given by

$$M_{sag} = \frac{wL^2}{8} + M_{hog} \tag{56}$$

Rearranging and substituting into Eq. (55) gives the rotation as

$$\theta_{sag} = -w\left[\frac{a_1}{L} - (a_2 + a_3)\frac{L}{8}\right] - M_{sag}\left(\frac{a_2+a_3}{L}\right) \tag{57}$$

Rearranging gives the UDL as

$$w = -\frac{\theta_{sag}L+M_{sag}(a_2+a_3)}{a_1-(a_2+a_3)\left(\frac{L^2}{8}\right)} \tag{58}$$

The elastic moment is then

$$M_{el} = \frac{wL^2}{24} = -\frac{L^2}{24}\left[\frac{\theta_{sag}L+M_{sag}(a_2+a_3)}{a_1-(a_2+a_3)\left(\frac{L^2}{8}\right)}\right] = \frac{\theta_{sag}L+M_{sag}\left[\frac{L^2}{2EI_{sag}}+\left(\frac{1}{EI_{hog}}-\frac{1}{EI_{sag}}\right)Lx_1\right]}{\frac{L^2}{2EI_{sag}}+\left(\frac{1}{EI_{hog}}-\frac{1}{EI_{sag}}\right)\left(3Lx_1-6x_1^2+\frac{4x_1^3}{L}\right)} \tag{59}$$

From Eq. (1), the MR factor is given by

$$K_{MR,sag} = \frac{1+\frac{M_{sag}}{\theta_{sag}}\left(\frac{1}{EI_{hog}}-\frac{1}{EI_{sag}}\right)\left(-2x_1+\frac{6x_1^2}{L}-\frac{4x_1^3}{L^2}\right)}{1+\frac{M_{sag}}{\theta_{sag}}\left[\frac{L}{2EI_{sag}}+\left(\frac{1}{EI_{hog}}-\frac{1}{EI_{sag}}\right)x_1\right]} \tag{60}$$

Similar expression can be derived for other loading conditions in the following form

$$K_{MR,sag} = \frac{1+\frac{M_{sag}}{\theta_{sag}}L\left(\frac{1}{EI_{hog}}-\frac{1}{EI_{sag}}\right)b_4}{1+\frac{M_{sag}}{\theta_{sag}}L\left[b_5\frac{1}{EI_{sag}}+\left(\frac{1}{EI_{hog}}-\frac{1}{EI_{sag}}\right)b_6\right]} \tag{61}$$

where the coefficients are given in Table 4. ξ can be approximated using the elastic points of contraflexure, resulting in the values in Table 5

Table 4 MR Coefficients for Hinge at Midspan

	$\mathbf{b_4}$	$\mathbf{b_5}$	$\mathbf{b_6}$
Continuous beam with equal end moments and UDL	$-2\xi + 6\xi^2 - 4\xi^3$	1/2	ξ
Continuous beam with equal end moments and central point load	$-\xi + 2\xi^2$	1/2	ξ
Propped cantilever with UDL	$-\frac{64}{27}\xi + \frac{64}{9}\xi^2 - \frac{64}{9}\xi^3 + \frac{64}{27}\xi^4$	32/27	$\frac{32}{9}\xi - \frac{32}{9}\xi^2 + \frac{32}{27}\xi^3$
Propped cantilever with central point load	$-\frac{6}{5}\xi + \frac{14}{5}\xi^2 - \frac{22}{15}\xi^3$	2/3	$2\xi - 2\xi^2 + \frac{2}{3}\xi^3$

Table 5 Approximate MR Coefficients for a Hinge at the Support

	$\mathbf{b_4}$	$\mathbf{b_6}$
Continuous beam with equal end moments and UDL (ξ =0.211)	-0.192	0.211
Continuous beam with equal end moments and central point load (ξ =0.25)	-0.125	0.25
Propped Cantilever with UDL (ξ =0.25)	-0.25	0.685
Propped Cantilever with Central Point Load (ξ =3/11)	-0.149	0.41

Upper limit on MR

If the hinge moment capacity has been reached at both supports and the midspan, additional moment redistribution cannot occur even if the rotation at these hinges is less than the rotational capacity and hence full MR is achieved. Setting $M_1=M_3=M_{hog}$ and $M_2=M_{sag}$ in Eq. (50), the uniformly distributed load is given as

$$w = \frac{8M_{sag}}{L^2} - \frac{8M_{hog}}{L^2} \tag{62}$$

The elastic moment at the support is then

$$M_{el} = -\frac{wL^2}{12} = -\frac{2}{3}M_{sag} + \frac{2}{3}M_{hog} \tag{63}$$

From Eq. (1), the MR factor at the support is

$$K_{MR,hog} = \frac{-\frac{2}{3}M_{sag} - \frac{1}{3}M_{hog}}{-\frac{2}{3}M_{sag} + \frac{2}{3}M_{hog}} \tag{64}$$

Similar expressions can be derived for other loading conditions in the following form

$$K_{MR,hog} = \frac{b_7 M_{sag} + b_8 M_{hog}}{b_7 M_{sag} + b_9 M_{hog}} \tag{65}$$

where b_7, b_8 and b_9 are given in Table 6.

Table 6 MR Coefficients for upper limit on MR

	b_7	**b_8**	**b_9**
Continuous Beam with UDL	-2	-1	2
Continuous Beam with Central Point Load	-1	-1	1
Propped Cantilever with UDL	-16	-9	6
Propped Cantilever with Central Point Load	-6	-5	3

Design Chart

Eq. (54) can be rewritten as

$$K_{MR,hog} = \frac{1+X(1-\alpha)b_1}{1+X[\alpha b_2+(1-\alpha)b_3]} \tag{66}$$

where

$$X = \frac{M_{hog}}{\theta_{hog}} \frac{L}{EI_{hog}} \tag{67}$$

and

$$\alpha = \frac{EI_{hog}}{EI_{sag}} \tag{68}$$

Similarly, Eq. (65) can be rewritten as

$$K_{MR,hog} = \frac{b_7-b_8\beta}{b_7-b_9\beta} \tag{69}$$

where

$$\beta = -\frac{M_{hog}}{M_{sag}} \tag{70}$$

From Eqs. (66) and (69) for specific combinations of α and β, K_{MR} can be plotted as a function of X in Fig. 8 that is similar to that by Visintin & Oehlers (2016). Note that α and β have been shown as equal as the stiffness is proportional to the strength for reinforced concrete members (Priestly et al. 2017). The curves are of a similar shape to the code expressions if X is assumed to be proportional to the neutral axis depth to effective depth ratio.

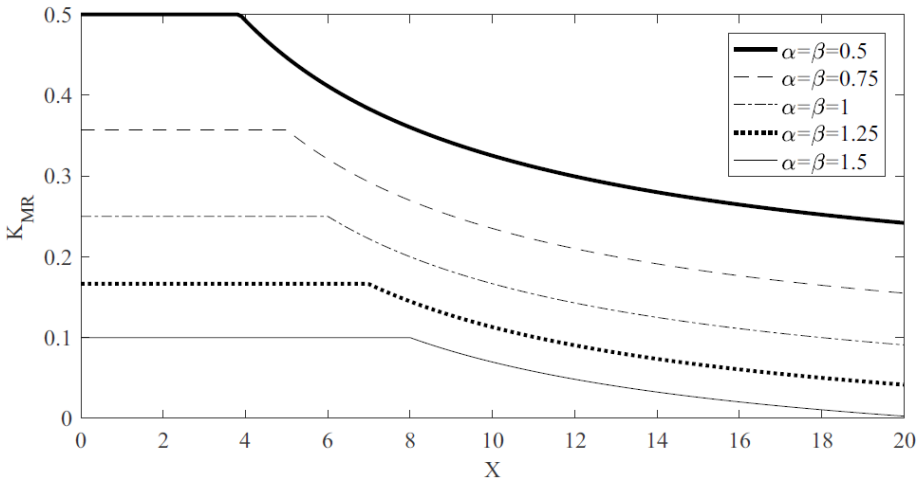

Fig. 8. Design Chart of Continuous Beam subjected to a UDL with constant end moments

COMPARISON TO EXPERIMENTAL RESULTS

The tests by do Carmo & Lopes (2004) and Scott & Whittle (2005) on two-span continuous beams are compared with the theory in Table 7 where: where the column labelled Pred. (Partial MR) refers to the MR estimated considering Partial MR as given by Eq. (66); while Pred. (full MR) refers to the MR obtained assuming full MR as given by Eq. (69).

The actual predicted K_{MR} value, which is in bold in Table 7, is the minimum of the partial and full interaction values. In all cases the beams reached full MR. This demonstrates the difficulty with trying to quantify MR with lab-scale specimens as these specimens tend to be quite ductile which makes partial MR behaviour difficult to explore. This also highlights the importance of the presented theory as this allows us to relate the MR to the rotational capacity which can be measured experimentally in a laboratory setting.

Table 7 Comparison to Test Results

Reference	Specimen	M_{hog}	M_{sag}	EI_{hog}	EI_{sag}	θ_{hog}	K_{MR}		M_h/M_{el}		
		kNm	kNm	$\times 10^9$ Nmm^2	$\times 10^9$ Nmm^2	radians	Exp.	Pred.	Exp.	Pred.	Exp./ Pred.

								Partial MR	Full MR			
do Carmo & Lopes (2004)	V1-0.8-0.7	20.2	44.3	921	1899	0.0187	0.39	0.53	**0.51**	0.61	0.49	1.24
	V1-0.8-1.4	38.4	44.3	1628	1899	0.0157	0.16	0.35	**0.19**	0.84	0.81	1.04
	V1-0.8-2.1	50.1	60.9	2149	2543	0.0173	0.35	0.38	**0.22**	0.65	0.78	0.83
	V1-0.8-2.9	66.6	89.5	2756	3519	0.0143	0.11	0.35	**0.28**	0.89	0.72	1.24
	V1-0.8-3.8	80.8	89.5	3233	3519	0.0109	0.05	0.25	**0.17**	0.95	0.83	1.14
	V1-0.8-5.0	98.3	89.5	3705	3519	0.0076	-0.02	0.15	**0.05**	1.02	0.95	1.07
Scott & Whittle (2005)	B2T12D	13.5	18	463	643	0.0503	0.27	0.65	**0.27**	0.73	0.73	1.00
	B2T12DX	13.5	18	463	643	0.0503	0.28	0.65	**0.27**	0.72	0.73	0.99
	B2T12DXX	13.5	18	463	643	0.0503	0.34	0.65	**0.27**	0.66	0.73	0.90
	B3T10D	13.6	18	479	643	0.0452	0.26	0.63	**0.27**	0.74	0.73	1.01
	B5T8D	16.1	18	504	643	0.0401	0.22	0.56	**0.18**	0.78	0.82	0.95
	B2T8E	8.2	11.4	232	329	0.0411	0.4	0.57	**0.29**	0.6	0.71	0.85
	B2T8EX	8.2	11.4	232	329	0.0411	0.55	0.57	**0.29**	0.45	0.71	0.63
	B2T20BH	74.3	105	4272	5949	0.0189	0.38	0.55	**0.3**	0.62	0.7	0.89
	B2T20BHX	74.3	105	4272	5949	0.0189	0.33	0.55	**0.3**	0.67	0.7	0.96
	B2T12DH	14.6	22.9	487	682	0.0394	0.4	0.59	**0.35**	0.6	0.65	0.92
	B2T12DHX	14.6	22.9	487	682	0.0394	0.45	0.59	**0.35**	0.55	0.65	0.85
											Mean	0.97
											Std. Dev.	0.15
											C.O.V.	0.16

The coefficients used in Eqs. (66) and (69) were given by the values for a propped cantilever with a central point load in Tables 3 and 6 where ξ =3/11 was assumed, which is the elastic point of contraflexure. The moment capacity, rotational capacity and flexural rigidity were evaluated using the numerical segmental model described in Visintin & Oehlers (2018). This approach can simulate concretes without fibres by setting the concrete tensile strength to zero after cracking. The material properties were taken from the published results or were estimated using the relationships in the fib Model Code 2010 (fib 2013).

The errors in Table 7 are presented in terms of M_h/M_{el} which is related to K_{MR} by rearranging Eq. (1) as follows

$$\frac{M_h}{M_{el}} = 1 - K_{MR} \tag{71}$$

M_h/M_{el} is also the parameter by which MR is represented in the fib Model Code 2010 (fib 2013). The reason for this is K_{MR} maybe positive or negative, therefore, the Exp./Pred. values can be difficult to interpret. For example if the predicted K_{MR} is small and positive while the experimental K_{MR} is small and negative this can result in a negative Exp./Pred. As M_h/M_{el} is distributed around 1 ensuring a positive value for Exp./Pred. the interpretation of the errors is more straightforward.

COMPARISON TO CODE APPROACHES

The parametric study in Fig. 9 compares Eq. (53) for full MR to code values that also apply to full MR. The moment capacity, rotational capacity and flexural rigidity of the beam were also calculated using the model in Visintin & Oehlers (2018). The default values in this study are: effective depth of 500 mm; concrete strength of 40 MPa; class N reinforcement; span-to-depth ratio of 20; continuous beam; and the stiffness of the hogging and sagging regions are the same. Each of these parameters are varied while the others are held constant as the influence of each parameter is explored. For all simulations, the hinges are also assumed to form at the supports as this is the usual case considered in the codes. All beams were also singly reinforced and the width was 200 mm, as these parameters were not found to significantly affect MR. For each case considered the reinforcement ratio was varied from 0.25% to 1% to produce the observed variation in neutral axis depth. The neutral axis depth was evaluated for a top strain of 0.003 as required by AS3600-2018 (Standards Australia 2018).

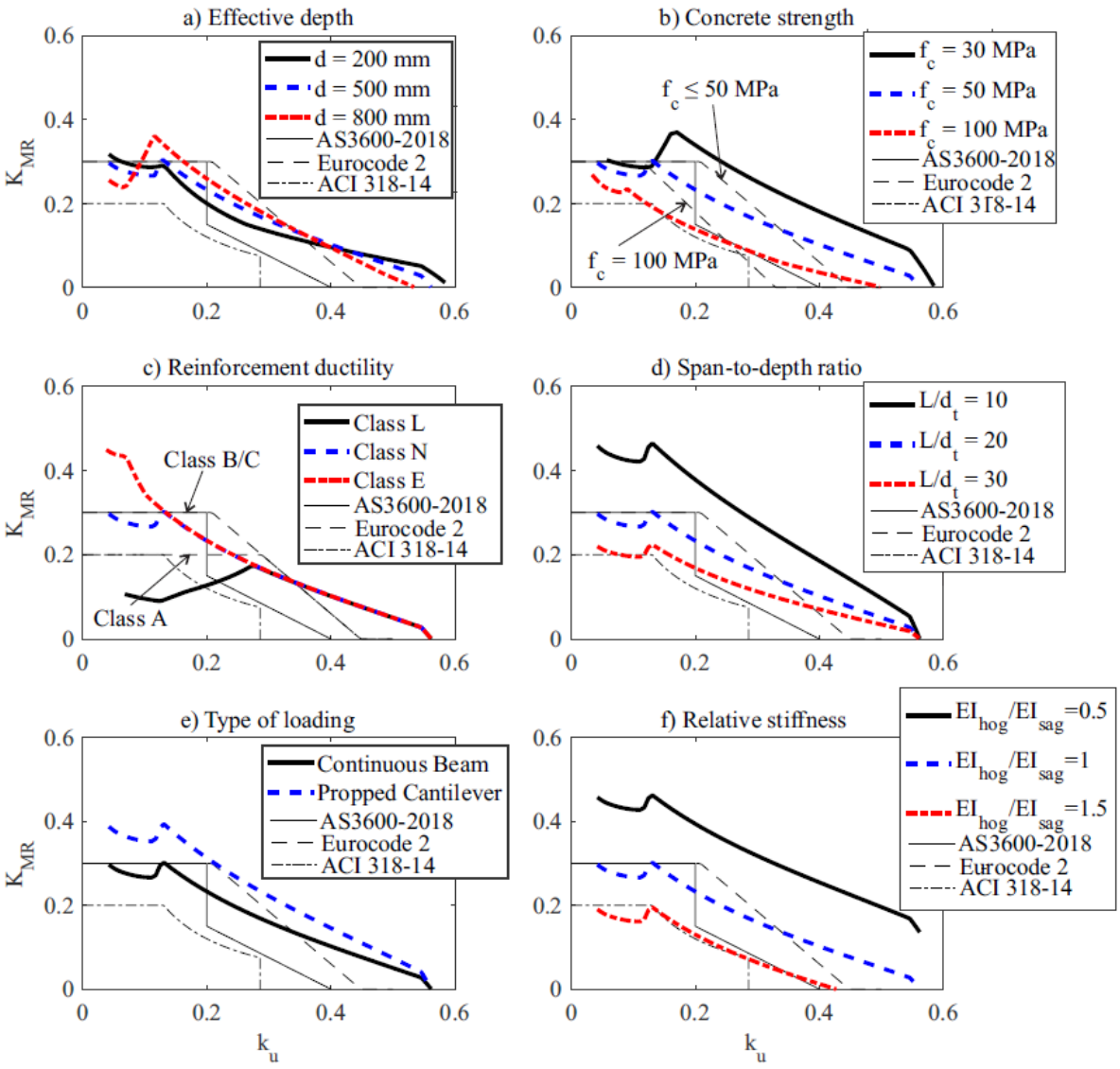

Fig. 9. Comparison to Code Approaches

From Fig. 9(a), it can be seen that the effective depth does not have a strong effect on the level of MR. This is because, even though the curvature is reduced, the size of the hinge increases with beam depth. However, the shape of the curve is different from that in the design codes. The initial branch of the curve is when the rotational capacity is controlled by the tensile failure of the reinforcement and the falling branch is when the rotational capacity is controlled by the crushing of the concrete. The rotational capacity of the section tends to increase with neutral axis depth when this parameter is controlled by the rupture of the reinforcement and the

rotational capacity decreases with neutral axis depth when this parameter is controlled by the crushing of the concrete.

In Fig. 9(b), increasing concrete strength results in a decrease in MR. This is consistent with the Eurocode 2 (CEN 2004) which reduces the allowable MR for concretes with a strength greater than 50 MPa.

Fig. 9(c) shows that an increased reinforcement ductility results in an increased level of MR for the cases where the rotational capacity is controlled by the rupture of the tensile reinforcement. However when concrete crushing controls the rotational capacity, the ductility of the reinforcement has no effect as would be expected. Eurocode 2 (CEN 2004) reduces the maximum level of MR to 0.2 for low ductility reinforcement while AS3600-2018 (Standards Australia 2018) does not allow MR to be considered for low ductility reinforcement. Note that in AS/NZS 4671-2001 (Standards Australia 2001) class E reinforcement has a minimum elongation of 0.1, while class N reinforcement has a minimum elongation of 0.05 and class L reinforcement has a minimum elongation of 0.015. Similarly, in the Eurocode 2 (CEN 2004), class A has a minimum elongation of 0.025, class B has a minimum elongation of 0.05 and class C has a minimum elongation of 0.075.

From Fig. 9(d), the level of MR decreases for beams with greater span to depth ratios. Fig. 9(e) demonstrates that more MR occurs for a propped cantilever than for a continuous beam. Fig. 9(f) found that the stiffer the sagging region is relative to the hogging region, the greater the expected MR is at the support.

From this parametric study, it can be seen that while existing code approaches consider the effect of concrete strength and reinforcement ductility on the MR, the influence of member properties such as span, type of loading and relative stiffness of the midspan and the support

are neglected. This suggests that the expressions in this paper could be used as the basis of design expressions which considers the effects of both section and member properties.

APPLICATION TO ULTRA-HIGH PERFORMANCE FIBRE REINFORCED CONCRETE

In Fig. 10, the predicted and experimental MR factors are compared for the UHPFRC beams tested by Visintin et al. (2018). The moment-rotation of these beams were recorded during the tests, hence, these results were used directly rather than from predictive models. It can be seen that the expressions in this paper give a close prediction of the MR. Importantly, to apply the approach to beams constructed from UHPFRC the only change is in the inputs to the model, not in the form of the model. To apply the approach to members where the moment-rotation relationship is unknown, approaches such as those by Schumacher (2006) or Sturm et al. (2020) which allow for tension stiffening and fibre bridging effects for fibre reinforced materials can be applied.

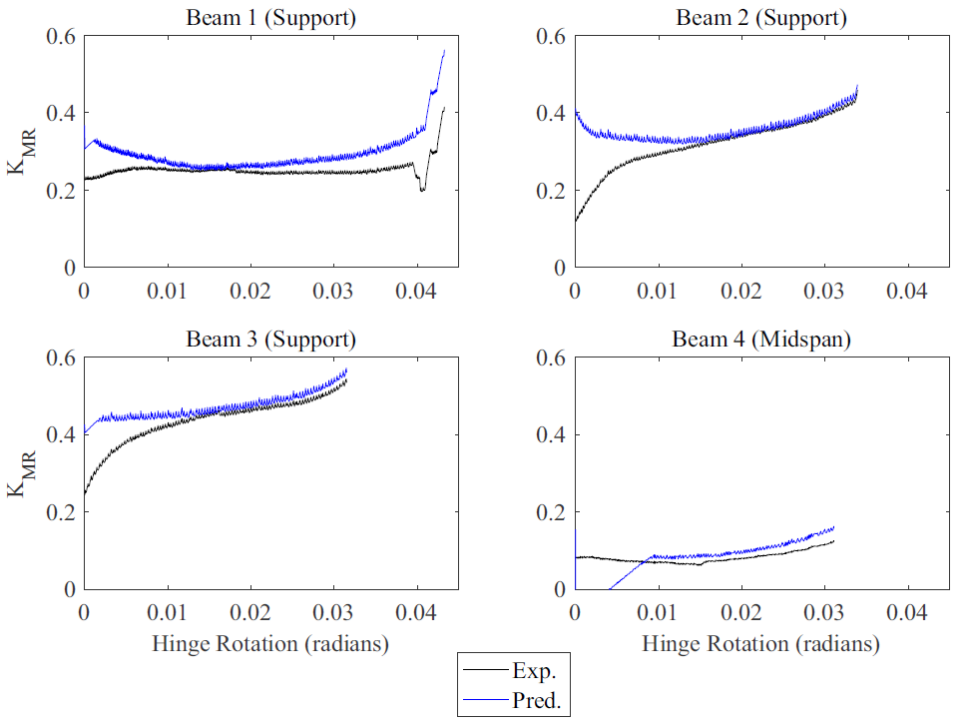

Fig. 10. Comparison of Experimental to Predicted MR for Visintin et al. (2018)

CONCLUSION

Mechanics expressions have been derived for the MR in reinforced concrete beams. These expressions allow the hinge rotation required to achieve full MR to be determined, that is the MR required to achieve the theoretical maximum load based on the sectional moment capacity of the beam. Expressions have also been developed for the maximum load that can applied if the rotational capacity of the hinges is insufficient to reach full MR, that is, partial MR is achieved. Finally, mechanics expressions are derived for the MR factors for a number of common design scenarios. These expressions are functions of the moment capacity of the hinges, rotational capacity of the hinges, flexural rigidity along the member, span of the beam, type of loading as well as the restraint conditions. Hence, these expressions can be applied for beams constructed from any combination of concrete and reinforcement as long as the value of these parameters can be defined.

The expressions are then validated against experimental results for conventional reinforced concrete beams as well as UHPFRC beams with good correlation, demonstrating the versatility of the solutions. Finally, a parametric study was performed comparing the results of using these expressions in national codes of practice to illustrate the importance of the different parameters effecting MR.

APPENDIX A CONTINUOUS BEAM WITH POINT LOAD

Consider the continuous beam in Fig. A1 which is subjected a point load, P, a distance a from the left hand support. It is subjected the distribution of moment as follows

$$M(x) = P\left(1 - \frac{a}{L}\right)x + M_1\left(1 - \frac{x}{L}\right) + M_3\left(\frac{x}{L}\right); 0 < x < a \quad \text{(A1a)}$$

$$M(x) = P\left(\frac{a}{L}\right)(L - x) + M_1\left(1 - \frac{x}{L}\right) + M_3\left(\frac{x}{L}\right); a < x < L \quad \text{(A1b)}$$

The elastic deflection at the right hand support is a superposition of the deflection due to the applied point load and the end moments. From Eq. (3) the curvature due to the point load is

$$\chi(x) = \frac{P}{EI_i}\left(1 - \frac{a}{L}\right) x; x_{i-1} < x < x_i; x < a; i \in (1, j) \quad \text{(A2a)}$$

$$\chi(x) = \frac{P}{EI_i}\left(\frac{a}{L}\right)(L - x); x_{i-1} < x < x_i; x > a; i \in (j, N) \quad \text{(A2b)}$$

where j is the segment in which the point load is contained defined as $x_j < a < x_{j+1}$.

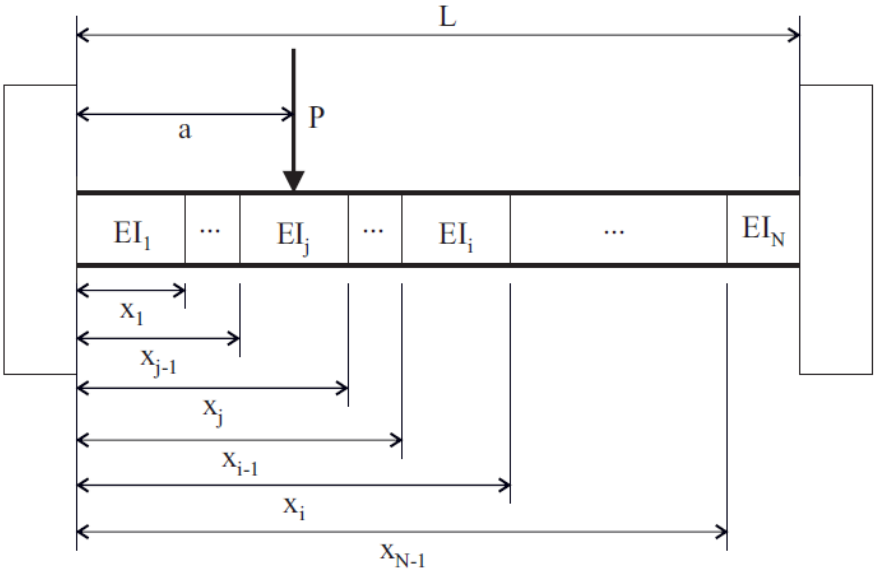

Fig. A1. Continuous Beam with Point Load

Integrating gives the rotation as

$$\theta_{el}(x) = \frac{P}{EI_i}\left(1 - \frac{a}{L}\right)\frac{x^2}{2} + (C_1)_i; x_{i-1} < x < x_i; x < a; i \in (1, j) \quad \text{(A3a)}$$

$$\theta_{el}(x) = \frac{P}{EI_i}\left(\frac{a}{L}\right)\left(Lx - \frac{x^2}{2}\right) + (C_2)_i; x_{i-1} < x < x_i; x > a; i \in (j, N) \quad \text{(A3b)}$$

At the left hand support the rotation is zero, therefore

$$\theta(0) = 0 = (C_1)_1 \quad \text{(A4)}$$

The rotation is continuous across segment boundaries, therefore from Eq. (A3a)

$$\theta(x_i) = \frac{P}{EI_i}\left(1 - \frac{a}{L}\right)\frac{x_i^2}{2} + (C_1)_i = \frac{P}{EI_{i+1}}\left(1 - \frac{a}{L}\right)\frac{x_i^2}{2} + (C_1)_{i+1} \quad \text{(A5)}$$

Rearranging gives

$$(C_1)_{i+1} - (C_1)_i = P\left(\frac{1}{EI_i} - \frac{1}{EI_{i+1}}\right)\left(1 - \frac{a}{L}\right)\frac{x_i^2}{2} \quad \text{(A6)}$$

From Eq. (A3b)

$$\theta(x_i) = \frac{P}{EI_i}\left(\frac{a}{L}\right)\left(Lx_i - \frac{x_i^2}{2}\right) + (C_2)_i = \frac{P}{EI_{i+1}}\left(\frac{a}{L}\right)\left(Lx_i - \frac{x_i^2}{2}\right) + (C_2)_{i+1} \quad \text{(A7)}$$

Rearranging gives

$$(C_2)_{i+1} - (C_2)_i = P\left(\frac{1}{EI_i} - \frac{1}{EI_{i+1}}\right)\left(\frac{a}{L}\right)\left(Lx_i - \frac{x_i^2}{2}\right) \quad \text{(A8)}$$

The rotation is also continuous at the point of loading so

$$\theta(a) = \frac{P}{EI_j}\left(1 - \frac{a}{L}\right)\frac{a^2}{2} + (C_1)_j = \frac{P}{EI_j}\left(\frac{a}{L}\right)\left(La - \frac{a^2}{2}\right) + (C_2)_j \quad \text{(A9)}$$

From which rearranging gives

$$(C_2)_j - (C_1)_j = -\frac{P}{EI_j}\frac{a^2}{2} \quad \text{(A10)}$$

Integrating Eq. (A3) gives the elastic deflection as

$$y_{el}(x) = \frac{P}{EI_i}\left(1 - \frac{a}{L}\right)\frac{x^3}{6} + (C_1)_i x + (C_3)_i; x_{i-1} < x < x_i; x < a; i \in (1, j) \quad \text{(A11a)}$$

$$y_{el}(x) = \frac{P}{EI_i}\left(\frac{a}{L}\right)\left(\frac{Lx^2}{2} - \frac{x^3}{6}\right) + (C_2)_i x + (C_4)_i; x_{i-1} < x < x_i; x > a; i \in (j, N) \quad \text{(A11b)}$$

The deflection is zero at the left hand support, therefore

$$y_{el}(0) = 0 = (C_3)_1 \quad \text{(A12)}$$

The deflection is also continuous across segment boundaries so from Eq. (A11a)

$$y_{el}(x_i) = \frac{P}{EI_i}\left(1 - \frac{a}{L}\right)\frac{x_i^3}{6} + (C_1)_i x_i + (C_3)_i = \frac{P}{EI_{i+1}}\left(1 - \frac{a}{L}\right)\frac{x_i^3}{6} + (C_1)_{i+1} x_i + (C_3)_{i+1} \quad \text{(A13)}$$

Rearranging gives

$$(C_3)_{i+1} - (C_3)_i = P\left(\frac{1}{EI_i} - \frac{1}{EI_{i+1}}\right)\left(1 - \frac{a}{L}\right)\frac{x_i^3}{6} - [(C_1)_{i+1} - (C_1)_i]x_i = -P\left(\frac{1}{EI_i} - \frac{1}{EI_{i+1}}\right)\left(1 - \frac{a}{L}\right)\frac{x_i^3}{3} \quad \text{(A14)}$$

From Eq. (A11b)

$$y_{el}(x_i) = \frac{P}{EI_i}\left(\frac{a}{L}\right)\left(\frac{Lx_i^2}{2} - \frac{x_i^3}{6}\right) + (C_2)_i x_i + (C_4)_i = \frac{P}{EI_{i+1}}\left(\frac{a}{L}\right)\left(\frac{Lx_i^2}{2} - \frac{x_i^3}{6}\right) + (C_2)_{i+1} x_i + (C_4)_{i+1} \quad \text{(A15)}$$

Rearranging gives

$$(C_4)_{i+1} - (C_4)_i = P\left(\frac{1}{EI_i} - \frac{1}{EI_{i+1}}\right)\left(\frac{a}{L}\right)\left(\frac{Lx_i^2}{2} - \frac{x_i^3}{6}\right) - [(C_2)_{i+1} - (C_2)_i]x_i = -P\left(\frac{1}{EI_i} - \frac{1}{EI_{i+1}}\right)\left(\frac{a}{L}\right)\left(\frac{Lx_i^2}{2} - \frac{x_i^3}{3}\right) \quad \text{(A16)}$$

The deflection is also continuous at the point load, so

$$y_{el}(a) = \frac{P}{EI_j}\left(1 - \frac{a}{L}\right)\frac{a^3}{6} + (C_1)_j a + (C_3)_j = \frac{P}{EI_j}\left(\frac{a}{L}\right)\left(\frac{La^2}{2} - \frac{a^3}{6}\right) + (C_2)_j a + (C_4)_j \quad \text{(A17)}$$

Rearranging gives

$$(C_4)_j - (C_3)_j = -\frac{P}{EI_j}\frac{a^3}{3} - \left[(C_2)_j - (C_1)_j\right]a = \frac{P}{EI_j}\frac{a^3}{6} \quad \text{(A18)}$$

The elastic deflection at the right hand support is then given by

$$y_{el}(L) = \frac{P}{EI_N}\frac{aL^2}{3} + (C_2)_N L + (C_4)_N = a_4 P \quad \text{(A19)}$$

where

$$a_4 = \frac{1}{EI_N}\frac{L^2 a}{3} + \frac{1}{EI_j}\left(-\frac{La^2}{2} + \frac{a^3}{6}\right) + \sum_{i=1}^{j-1}\left(\frac{1}{EI_i} - \frac{1}{EI_{i+1}}\right)\left(1 - \frac{a}{L}\right)\left(\frac{Lx_i^2}{2} - \frac{x_i^3}{3}\right) + \sum_{i=j}^{N-1}\left(\frac{1}{EI_i} - \frac{1}{EI_{i+1}}\right)\left(\frac{a}{L}\right)\left(L^2 x_i - Lx_i^2 + \frac{x_i^3}{3}\right) \quad \text{(A20)}$$

Hence the total elastic deflection at the right hand support for a continuous beam with a point load is given by

$$y_{el}(L) = a_4 P + a_2 M_1 + a_3 M_3 \quad \text{(A21)}$$

Similarly the elastic deflection at the left hand support

$$y_{el}(0) = a_4' P + a_2' M_1 + a_3' M_3 \quad \text{(A22)}$$

where

$$a_4' = \frac{1}{EI_1}\left(1 - \frac{a}{L}\right)\frac{L^3}{3} + \frac{1}{EI_j}\left[\frac{(L-a)^3}{6} - \frac{L(L-a)^2}{2}\right] - \sum_{i=1}^{j-1}\left(\frac{1}{EI_i} - \frac{1}{EI_{i+1}}\right)\left(\frac{a}{L}\right)\left(\frac{L(x_i')^2}{2} - \frac{(x_i')^3}{3}\right) - \sum_{i=j}^{N-1}\left(\frac{1}{EI_i} - \frac{1}{EI_{i+1}}\right)\left(1 - \frac{a}{L}\right)\left(L^2 x_i' - L(x_i')^2 + \frac{(x_i')^2}{3}\right) \quad \text{(A23)}$$

Using the results of Eqs. (A21) and (A22) hinges locations can then be determined using Table 1. The rotation at these hinges can then be determined from Eqs. (29)-(34), choosing the appropriate expressions based on the hinge locations.

NOTATION

The following symbols are used in this paper:

a = position of point load with respect to left hand support;

$a_1, a_2, a_3, a_4, a_1', a_2', a_3', a_4'$ = coefficients for the rotational demand;

$b_1, b_2, b_3, b_4, b_5, b_6, b_7, b_8, b_9$ = coefficients for moment redistribution expression;

$(C_1)_i$, $(C_2)_i$, $(C_3)_i$, $(C_4)_i$ = integration coefficients; EI = flexural rigidity;

EI_{hog}, EI_{sag} = flexural rigidity in the hogging and sagging regions, respectively;

EI_i = flexural rigidity of i^{th} segment;

EI_1, EI_2, EI_3 = flexural rigidity of the leftmost hogging region, sagging region and rightmost hogging region;

f_c = concrete strength;

K_{MR}, $K_{MR,hog}$, $K_{MR,sag}$ = moment redistribution; moment redistribution at support and at the position of maximum sagging moment, respectively;

k_u = ratio between neutral axis and effective depth;

L = span;

L_h = length of hinge;

M, M_{el}, M_h = moment; elastic and hinge moments, respectively;

M_{hog}, M_{sag} = moments at the support in the hogging region and postion of maximum sagging moment, respectively;

M_{st}, $(M_{st})_{el}$, $(M_{st})_{FMR}$, $(M_{st})_{PMR}$ = static moment; elastic static moment; static moment at full MR; static moment at partial MR;

M_1, M_2, M_3 = moments at the left hand support, position of maximum sagging moment and right hand support, respectively;

N = number of segments;

P = point load;

w = uniformly distributed load;

X = moment redistribution parameter;

x = position with respect to the left hand support;

x' = position with respect to the right hand support;

x_i = distance from left hand support to the left hand boundary of i^{th-} segment

x_m = distance from left hand support to point of maximum moment;

y, y_{el}, y_h = deflection; elastic and hinge deflections, respectively;

α = ratio of flexural rigidity of the hogging to the sagging region;

β = ratio of moment capacity at the support to the moment capacity at the position of maximum sagging moment;

ε_u = ultimate concrete strain;

θ_{cap} = rotation capacity;

θ_{el}, θ_h = elastic rotation;hinge rotation;

θ_{hog}, θ_{sag} = rotation at support in hogging region and at position of maximum sagging moment, respectively;

θ_1, θ_2, θ_3= hinge rotations at the left hand, position of maximum sagging moment and right hand supports, respectively;

ξ = ratio of distance to the point of contraflexure with respect to the left hand support to the span of the beam;

χ = curvature;

REFERENCES

ACI (American Concrete Institute) (2014) *Building code requirements for structural concrete. ACI 318-14.* American Concrete Institute, Farmington Hills, Michigan.

Bachmann, H. (1971). Influence of shear and bond on rotational capacity of reinforced concrete beams. *Institut fur Baustatik ETH Zurich*, 36, 11-27

Bigaj. A.J. (1999). *Structural dependence of rotational capacity of plastic hinges in RC beams and slabs*. (Ph.D. Thesis, Delft University of Technology, Delft, Netherlands).

CEN (European Committee for Standardisation) (2004). Eurocode 2: *Design of concrete structures - Part 1-1: General rules and rules for building. EN 1992-1-1:2004.* European Committee for Standardisation, Brussels, Belgium.

Do Carmo, R. N., & Lopes, S. M. (2005). Ductility and linear analysis with moment redistribution in reinforced high-strength concrete beams. *Canadian Journal of Civil Engineering*, 32(1), 194-203.

Drucker, D. C., Prager, W., & Greenberg, H. J. (1952). Extended limit design theorems for continuous media. *Quarterly of applied mathematics*, 9(4), 381-389.

fib (International Federation for Structural Concrete) (2013). *fib Model Code for Concrete Structures 2010*. Ernst & Sohn, Berlin, Germany.

Gravina, R.J. (2002) *Non-linear overload behaviour and ductility of reinforced concrete flexural members containing 500MPa grade steel reinforcement.* (Ph.D. Thesis, University of Adelaide, Adelaide, Australia).

Gravina, R. J., & Warner, R. F. (2003). Evaluation of the AS 3600 design clauses for moment redistribution and minimum ductility levels. *Australian Journal of Structural Engineering*, 5(1), 37-45.

Haskett, M., Oehlers, D. J., Ali, M. M., & Wu, C. (2009). Rigid body moment–rotation mechanism for reinforced concrete beam hinges. *Engineering Structures*, 31(5), 1032-1041.

Panagiotakos, T. B., & Fardis, M. N. (2001). Deformations of reinforced concrete members at yielding and ultimate. *ACI Structural Journal*, 98(2), 135-148.

Priestly, M.J.N, Calvi, G.M., & Kowalsky, M.J. (2017). *Displacement-based seismic design of structures.* Fondazione Eucentre, Pavia, Italy.

Schumacher, P. (2006) *Rotation capacity of self-compacting steel fiber reinforced concrete.* (Ph.D. Thesis, Delft University of Technology, Delft, Netherlands).

Scott, R. H., & Whittle, R. T. (2005). Moment redistribution effects in beams. *Magazine of concrete research*. 57(1), 9-20.

Standards Australia (2001). *Steel reinforcing materials. AS/NZS4671:2001*. Standards Australia, Sydney, Australia.

Standards Australia (2018). *Concrete Structures. AS3600:2018*. Standards Australia, Sydney, Australia.

Sturm, A.B., Visintin, P. & Oehlers. D.J. (2019) Blending fibres to enhance the flexural properties of UHPFRC beams. *Construction and Building Materials*, in press.

Visintin, P., & Oehlers, D. J. (2016). Mechanics-based closed-form solutions for moment redistribution in RC beams. *Structural Concrete*, 17(3), 377-389.

Visintin, P., Mohamed Ali, M.S., Xie, T. & Sturm, A.B. (2018) Experimental investigation of moment redistribution in ultra-high performance fibre reinforced concrete beams. *Construction & Building Materials*, 166(1), 433-444.

Visintin, P., & Oehlers, D. J. (2018). Fundamental mechanics that govern the flexural behaviour of reinforced concrete beams with fibre-reinforced concrete. *Advances in Structural Engineering*, 21(7), 1088-1102.